Power-Law Scaling Relating the Average Charge State and Kinetic Energy in Expanding Laser-Driven Plasmas

J. Sheil,[1,2,*] L. Poirier,[1,2] A. C. Lassise,[1] D. J. Hemminga,[1,2] S. Schouwenaars,[1,3] N. Braaksma,[4] A. Frenzel,[4] R. Hoekstra,[1,5] and O. O. Versolato[1,2]

[1]*Advanced Research Center for Nanolithography, Science Park 106, 1098 XG Amsterdam, The Netherlands*
[2]*Department of Physics and Astronomy, and LaserLaB, Vrije Universiteit Amsterdam, De Boelelaan 1081, 1081 HV Amsterdam, The Netherlands*
[3]*Department of Applied Physics, Eindhoven University of Technology, Den Dolech 2, 5600 MB Eindhoven, The Netherlands*
[4]*ASML US LP, 17075 Thornmint Ct, San Diego, California 92127, USA*
[5]*Zernike Institute for Advanced Materials, University of Groningen, Nijenborgh 4, 9747 AG Groningen, The Netherlands*

(Received 28 February 2024; accepted 22 July 2024; published 17 September 2024)

A universal power-law scaling $\bar{z} \propto E^{0.4}$ in the correlation between the average ion charge state $\bar{z}$ and kinetic energy E in expanding laser-driven tin plasmas is identified. Universality here refers to an insensitivity to all experimental conditions: target geometry, expansion direction, laser wavelength, and power density. The power law is accurately captured in an analytical consideration of the dependence of the charge state on temperature and the subsequent transfer of internal to kinetic energy in the expansion. These analytical steps are individually, and collectively, validated by a two-dimensional radiation-hydrodynamic simulation of an expanding laser-driven plasma. This power-law behavior is expected to hold also for dense plasma containing heavier, complex ions such as those relevant to current and future laser-driven plasma light sources.

DOI: 10.1103/PhysRevLett.133.125101

Introduction—The characterization and manipulation of high-energy ions bred in laser-produced plasmas (LPPs) form a broad field of inquiry. For instance, the irradiation of tens-of-nanometers-thin targets with high-intensity laser radiation ($I > 10^{18}$ W cm^{-2}) generates massive electric fields $\sim$TV m^{-1} that can drive particle acceleration to kinetic energies $\sim$100 MeV [1–3]. Advancing our control of such particle beams (e.g., their energy spectrum and spatial distribution) may propel developments in fusion research [4], warm-dense-matter studies [5], and biomedical research [6,7]. A comprehensive understanding of plasma expansion dynamics is also crucial for studies utilizing lower-intensity laser light, such as laboratory investigations of magnetic reconnection [8], nuclear excitation studies [9,10], thin film deposition [11–13], and plasma-based light sources [14–16].

A key observable in plasma expansion studies is the charge-state-resolved ion kinetic energy distribution $d^2N_z/dEd\Omega$, which quantifies the number of ions N_z of charge state z per unit kinetic energy E per solid angle Ω. This distribution encodes a wealth of information on the fundamental processes occurring in the (expanding) plasma, and is relevant to numerous scientific fields and technological applications. In the pertinent example of LPP extreme ultraviolet (EUV) light sources for nanolithography, high-energy ions emanating from the dense plasma may damage sensitive optical components in lithography machines if not properly mitigated [17]. A detailed understanding of the strongly anisotropic ion kinetic energy distribution [18–20] is thus key for designing strategies, e.g., using buffer gas flow, to mitigate high-energy ions [21–24].

Once the ion kinetic energy distribution is known, important relations can be deduced, such as the relation between average charge state ($\bar{z}$) and kinetic energy or, equivalently, the location of the maxima of the distributions ($z_{\max}$) in kinetic energy space. Experiments show that, on average, higher charge states exhibit higher kinetic energies [25,26]. Put simply, the highest charge states are bred in the hottest and densest (and therefore highest-pressure) plasma regions, and spatial gradients in the electron pressure ∇p_e drive ion acceleration [27]. Although the recombination of free electrons with ions occurs throughout the expansion, complete neutralization of the plasma is typically inhibited by the strong density reduction inherent to the expansion. This effect is known as charge-state freezing [28,29]. Remarkably, given all the complex processes that can occur in the expansion, both $z_{\max}$ and $\bar{z}$ typically increase rather smoothly with increasing E. While such a correlation

*Contact author: sheil@arcnl.nl

has been identified for plasma produced from a wide range of elements under various conditions [30–36], its origin lacks a clear consensus and quantitative formulation in terms of basic plasma parameters.

In this Letter, we report on the identification of a universal power-law scaling $\bar{z} \propto E^{0.4}$ of the average ion charge state $\bar{z}$ with kinetic energy E in experiments on expanding laser-driven tin plasmas. The law is universal in the sense that it holds true irrespective of target geometry (tin droplet and disk targets), laser parameters (power density and laser wavelength), or expansion direction. The power law originates from a simple analytical relation between the average charge state (in hot and dense plasma regions) and the local plasma temperature, a claim that is supported by a two-dimensional radiation-hydrodynamic simulation of an expanding LPP. Our conclusions are furthermore shown to be more broadly applicable to dense plasmas containing heavier, complex ions that (i) exhibit a smooth increase of ionization potential with charge state z (open $4d$ subshell ions, for instance) and (ii) are produced in conditions close to local thermodynamic equilibrium (LTE).

Experiments and power-law behavior—In the first series of experiments, plasma expansion from laser-irradiated tin microdroplet targets was investigated. This choice was motivated by their role in LPP EUV sources for nanolithography and metrology applications [16,37]. A simplified schematic of the experiment is shown in Fig. 1(a) (see Ref. [38] for additional details). In these experiments, Nd:YAG laser pulses of wavelength $\lambda = 1.064$ μm and intensity $I \sim 10^{11}$ W cm^{-2} were incident on 27-μm-diameter tin microdroplets. Both the spatial and temporal laser profiles were Gaussian shaped with full-width-at-half-maximum values of 100 μm and 10 ns, respectively. Absolutely calibrated, charge-state-resolved ion kinetic energy distributions were recorded using a four-grid retarding-field analyzer (RFA) [39] positioned under an angle $\alpha = 30°$ with respect to the incident laser beam axis. The detector was placed a distance $d \approx 420$ mm away from the droplet target. The measured charge-state-resolved distributions are shown in Fig. 1(b). The charge-state-integrated distribution, obtained by summing the charge-state-resolved distributions, is shown by the black dashed line.

A few important observations can be made from Fig. 1(b) directly. First, the peak in the charge-state-integrated distribution located near 2 keV originates from a fast-moving blast shell formed in the early stages of the expanding plasma [20,27]. Second, a clear shift of the z-specific distributions to higher kinetic energies with increasing z is observed. From these distributions, the kinetic-energy-dependent average charge state $\bar{z}$ is calculated and is shown by the smooth red solid curve. This curve overlaps with the maxima of the charge-state-resolved distributions $z_{\max}$ (represented by open markers), but presents instead a continuous distribution over the entire detected energy range. Third, and perhaps most remarkable, $\bar{z}$ exhibits a power-law-like dependence on E of the form $\bar{z} \propto E^{0.4}$.

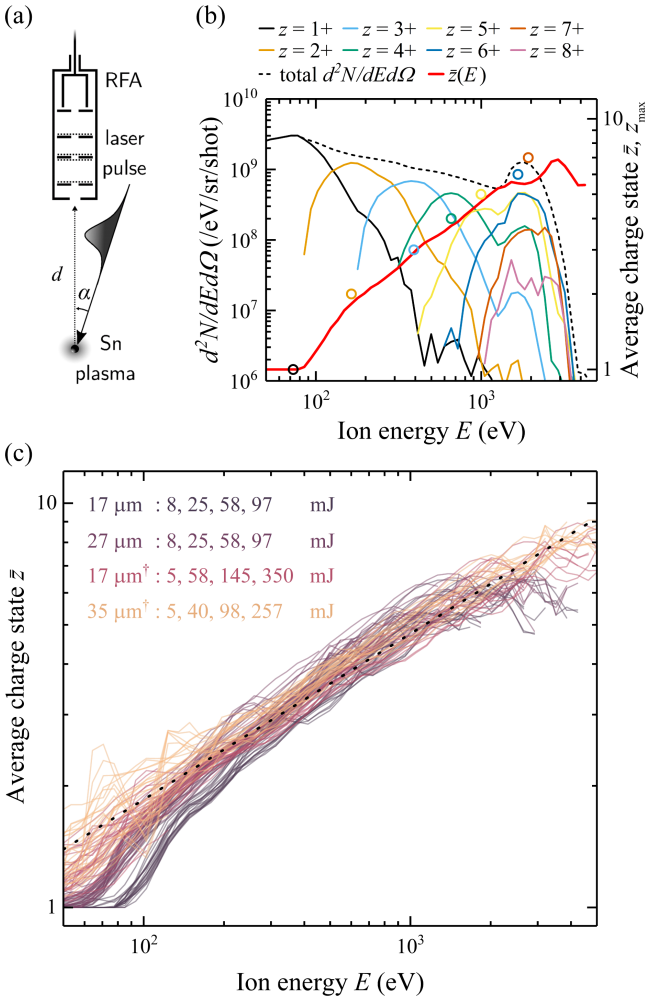

FIG. 1. (a) Simplified schematic of the experimental setup. Ion kinetic energy distributions were recorded using a four-grid RFA placed under an angle $\alpha = 30°$ with respect to the incident laser beam axis and positioned a distance $d \approx 420$ mm away from the LPP. (b) Charge-state-resolved distributions are shown as colored lines, and the black dashed line represents the charge-state-integrated distribution. The solid red curve represents the average charge state $\bar{z}$, and the open colors indicate the maxima of the charge-state-resolved spectra $z_{\max} \in \mathbb{N}$ (note that the $z = 8+$ distribution here does not feature a clear single maximum, and thus is omitted). (c) 112 $\bar{z}$ traces from experiments involving three droplet diameters (17, 27, and 35 μm), various laser intensities, multiple observation angles, and two laser pulse durations. Datasets labeled with a dagger (†) used a Gaussian laser pulse of duration 8 ns (10 ns otherwise). A collective power-law fit of $\bar{z} = 0.3E^{0.4}$ to the data is shown by the black dotted line.

To elucidate whether this power law is a more general phenomenon, we performed a second, more extensive series of experiments. The parameter space was extended to include three droplet sizes (17, 27, and 35-μm diameter) and laser intensities in the range $I = 0.4\text{–}40 \times 10^{10}$ W cm^{-2} [38]. The ion kinetic energy distributions were recorded under seven observation angles $\alpha = 30$, 41, 64, 90, 120, 139, and 150°. All in all, 112 $\bar{z}$ traces are shown in Fig. 1(c).

Remarkably, the power-law dependence of $\bar{z}$ on E holds irrespective of laser energy, droplet size, or detection angle. A global fit through these data, shown by the black dotted line, gives a relation of the form $\bar{z} = 0.3E^{0.4}$. Before expanding the scope of our experimental investigations further, we turn our attention to explaining the physical origin of this power law.

Analytical considerations and radiation-hydrodynamic simulation—It is instructive to first consider basic analytical arguments. The average charge state $\bar{z}$ established in hot and dense plasma regions originates from a complex interplay of density- and temperature-dependent collisional and radiative processes [40]. Although its calculation is best done using atomic kinetics modeling, simplified approaches can, in certain circumstances, yield accurate estimates [41]. For instance, starting with the Saha equation for ionization balance, and assuming that the ionization potential scales with the square of the charge state, Drake [42] derives a simple relation of the form $\bar{z} \sim \sqrt{T}$. A similar power-law dependence is also predicted by the Thomas-Fermi (TF) model [43] (see the Supplemental Material [44]), which, as shown in Ref. [48], predicts for tin plasmas $\bar{z} \propto T^{0.6}$ in the mass density and temperature ranges $10^{-4} \leq \rho \leq 10^{-2}$ g cm^{-3} and $10 \leq T \leq 100$ eV, respectively. The TF model is a semiclassical statistical theory of the atom that can provide reliable predictions for $\bar{z}$ for heavy ions away from closed-shell configurations [41], e.g., the current case of complex open-shell ions. We note that detailed comparisons of full-scale atomic calculations (see review in Ref. [49]) with the TF model support the $\bar{z} \propto T^{0.6}$ scaling. Next, following Murakami and Basko [50], we posit that the obtainable kinetic energy of the species scales with the product $\bar{z}T$; the kinetic energy at the sonic surface (that is, where the flow speed is equal to the sound speed c_s) is $E_{ss} = m_{\text{ion}}c_s^2/2 = \bar{z}T/2$, and the asymptotic (time $t \to \infty$) "bulk" kinetic energy of a spherical, adiabatic expansion takes the form $E_b = 4E_{ss} = 2\bar{z}T$ [50]. Combining these relations with the aforementioned $\bar{z} \propto T^{0.6}$ scaling yields the relationship $\bar{z} \propto E^{0.4}$, which has the same power 0.4 as that deduced from the experimental data presented in Fig. 1(c).

To further investigate the origin of this power law, we performed a two-dimensional axisymmetric radiation-hydrodynamic simulation of a laser-driven plasma expansion using the RALEF-2D code [51–53]. This code solves the equations of single-fluid, single-temperature hydrodynamics accounting for processes of thermal conduction, radiation transport, and laser energy deposition. We have utilized this code extensively in our previous studies on laser-plasma interaction [20,27,54], and we refer the reader to these works for additional details. Of importance to the current work is the calculation of cell-specific, density- and temperature-dependent $\bar{z}$ values. Following our previous studies, we calculated $\bar{z}$ according to the TF model as per the Frankfurt equation-of-state model [55–57]. As the code utilizes a single-fluid, single-temperature approach, quasi-neutral plasma expansion is driven by gradients in the pressure $\nabla p = \nabla(p_e + p_{\text{ion}}) \propto \nabla(n_{\text{ion}}k_B T[\bar{z} + 1])$, which is determined in large part by the average charge state $\bar{z}$ (p_{ion} and n_{ion} are the ion pressure and ion density, respectively). We note that in the single-fluid picture, a straightforward connection exists between the concepts of pressure and electric field $\mathcal{E}$ via $\mathcal{E} = -(en_e)^{-1}\nabla p_e$ [58,59]. The simulation results presented in the following represent the Nd:YAG-laser illumination of a 27 μm-diameter droplet with a laser pulse energy of 97 mJ.

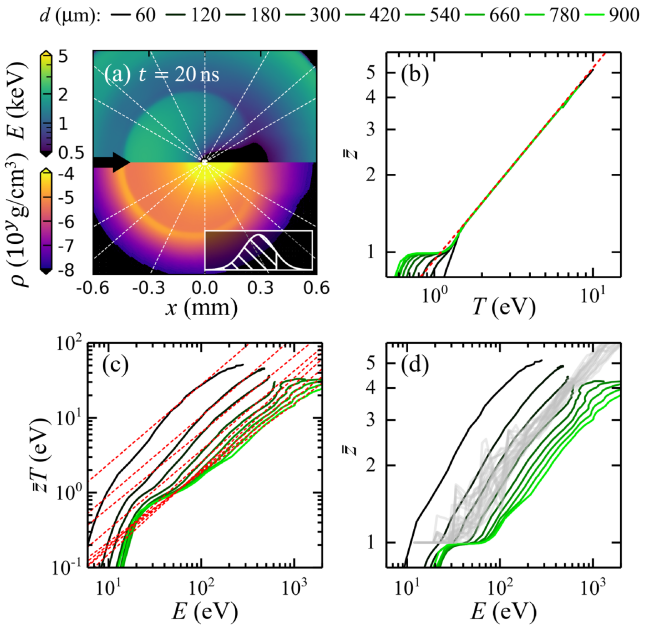

FIG. 2. (a) Two-dimensional RALEF-2D simulation results showing kinetic energy E (upper panel) and density ρ (lower panel) of the expanding plasma. Presented data correspond to 20 ns after laser pulse initiation. The shaded area in the inset illustrates the fraction of the total laser energy added to the system up to this time. The laser pulse propagates from left to right as indicated by the black arrow. (b) $\bar{z}$ vs T, (c) $\bar{z}T$ vs E, and (d) $\bar{z}$ vs E scalings obtained at different distances d from the center of the simulation mesh (black to green color scale; see top legend) at an observation angle $\alpha = 30°$ with respect to the x axis. Selected experimental data from Fig. 1(c) (35 μm-diameter droplet case) are overlaid as transparent gray lines. The red dashed line in panel (b) represents a single collective power-law fit to the data, and the red dashed lines in (c) represent power-law fits for each presented trace.

In Fig. 2(a) we show a two-panel color map of the kinetic energy E (upper panel) and mass density ρ (lower panel) of the plasma 20 ns after initiation of the laser pulse. This time frame corresponds to a few nanoseconds after the maximum intensity of the Gaussian laser pulse, as illustrated in the inset of the lower panel. As in our previous works [20,27], we note the existence of a high-kinetic energy ($E \approx 2$ keV) blast shell of radius ~0.5 mm, which is ultimately responsible for the high-energy "hump" observed in the experimental ion kinetic energy distribution

shown in Fig. 1(b). Its presence or absence however does not impact the following.

To investigate the validity of the simplified analytical approach relating $\bar{z}$ with E described above, we place imaginary "ion detectors" in our computational mesh at various distances d from the center of the droplet at an angle $\alpha = 30°$ with respect to the x axis, i.e., the laser axis. We then record $\bar{z}$ at the detector at each instant in time, and finally integrate the simulation results over the full expansion time (1 μs) to investigate a potential correlation between $\bar{z}$ and E as a function of radial distance d (d ranges from 60 to 900 μm). Figure 2(b) shows the results of the in-mesh detection approach in terms of the correlation between $\bar{z}$ and T, which is found to follow a power law (red dashed line) to high accuracy at all distances.

Next, we compare in Fig. 2(c) the quantities $\bar{z}T$ and E. The correlation is shown to indeed follow a common power law $E \propto \bar{z}T$ as indicated by straight-line fits to the data (red dashed lines), with prefactors that reduce with increasing distance d. This change in prefactor can be understood in terms of the continuous exchange between internal and kinetic energy throughout the expansion. At peak intensity, the kinetic energy at the sonic surface ($d \approx 20$ μm) is $E_{ss} = \bar{z}T/2 \approx 375$ eV, which translates to a final kinetic energy of $E \approx 2$ keV as seen in Fig. 2(c). This value is in reasonable agreement with the aforementioned bulk kinetic energy of an adiabatic expansion $E_b = 2\bar{z}T \approx 1.5$ keV. Finally, in Fig. 2(d) we present the sought-after correlation between $\bar{z}$ and E overlayed with a selection of experimental results (transparent gray lines). The power-law behavior immediately stands out and is found to accurately reproduce the experimental data at distances between 120 and 300 μm. Here, as in Fig. 2(c), the prefactor of the power law from the simulations decreases with increasing distance d. At a certain distance $d \approx 300$ μm the simulation drops below the experimental correlation, which reflects the fact that our simulations cannot reliably predict the average charge state; the TF model cannot reproduce non-equilibrium effects associated with charge-state freezing [28,29,60]. We now want to demonstrate that beyond $d \approx 300$ μm, $(d\bar{z}/dt)_{\text{RALEF-2D}} \gg (d\bar{z}/dt)_{\text{reality}}$. On the one hand, our RALEF-2D simulations indicate a $d\bar{z}/dt$ of several 10^8 s^{-1} for $d = 100$–300 μm. On the other hand, Badnell *et al.* [61] and, separately, Fu *et al.* [62] demonstrated that dielectronic recombination (DR) is the dominant recombination mechanism in these conditions, with DR rate coefficients at the level of, for example, $\sim 10^{-10}$ cm^3/s for $z = 4+$. The RALEF-2D TF-model-implied rate can thus be "supported" by DR at an electron density of 10^{18} e^-/cm^3, the isosurface of which lies approximately 100 μm from the droplet surface. At 10^{17} e^-/cm^3, however, with its isosurface near 300 μm, the $d\bar{z}/dt$ rate implied by RALEF-2D is 1 order of magnitude higher than can be supported by DR, the dominant recombination mechanism. At this point, the TF model breaks down, and given the fast drop in density with increasing distance, charge state freezing will ensue. The agreement between simulation and experiment is strikingly good for $d = 120$–300 μm and underpins the validity of the proposed relation $\bar{z} \propto E^{0.4}$.

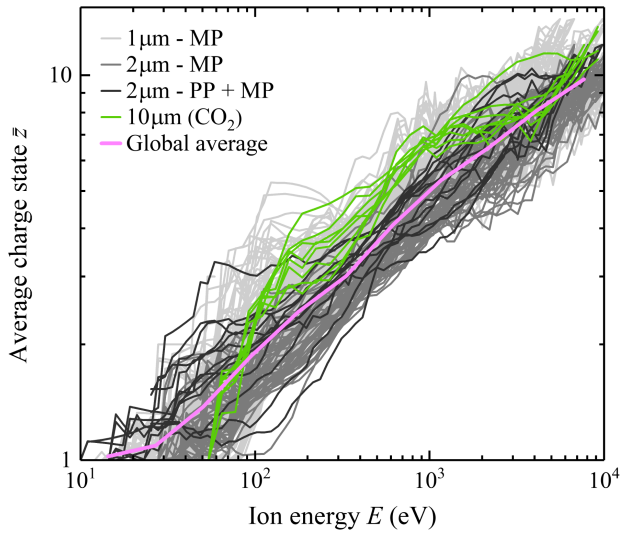

FIG. 3. $\bar{z}$ traces recorded in a large parameter space (see the Supplemental Material [44]). The datasets are separated into four categories: (i) 1 μm-wavelength main pulse (MP) only (light gray lines), (ii) 2 μm-wavelength MP only (gray lines), (iii) combined 1 μm prepulse (PP) and 2 μm MP (dark gray lines), and (iv) 10 μm-wavelength (CO_2 MP (green lines)). The averaged $\bar{z}$ trace is shown as the pink line. A power-law fit to this trace (not shown) gives a relation $\bar{z} \propto E^{0.37}$.

Generalization—Having explained the origin of the experimentally observed power-law behavior $\bar{z} \propto E^{0.4}$ both from simplified analytical arguments and numerical simulation, one can now ask whether the scaling holds over a broader range of experimental conditions. In Fig. 3 we present data taken from various LPPs (see Table S1 in the Supplemental Material [44]), ranging from plasma generated with various drive laser wavelengths (1, 2, and 10.6 μm-driven plasmas), over plasma generated from droplet as well as preshaped disk targets, to CO_2-laser-driven plasma (of much lower density [17]) similar to those currently used in the industry. The averaged $\bar{z}$ trace, represented by the pink line, also shows clear power-law-like behavior. Clearly, we see that power-law behavior is common to all of these plasmas, the origin of which traces to a relation linking average charge state to plasma temperature $\bar{z} \propto T^{0.6}$.

This realization invites an extension to dense plasmas of elements heavier than Sn. TF calculations (see the Supplemental Material [44]) of such elements, and specifically to conditions where open $4f/4d$ subshell ions are produced, also exhibit power-law relations of the form $\bar{z} \propto T^{0.6}$, a surprising universality of the relation. The heavy elements Gd and Tb are of prime interest for beyond-EUV

lithography (at 6.7 nm) where the light originates from transitions within complex open $4d$ and $4f$ subshell ions (e.g., charge states 18–27+) [63–65]. Plasmas containing highly charged Au, Pb, and Bi ions (charge states up to 40+) are candidate light sources for biological imaging in the water window region (2.3–4.4 nm) [66,67]. Based on the $\bar{z} \propto T^{0.6}$ scaling, we propose that the $\bar{z} \propto E^{0.4}$ (the power exponent deriving from $0.6/1.6 \approx 0.4$) relation holds for the complete "quasi-Moseley" curve [68], which relates $\Delta n = 0$, $n = 4 - n = 4$ emission wavelength to element, ranging from tin (13.5 nm) to bismuth (4 nm).

Conclusions—We have presented a universal power-law scaling $\bar{z} \propto E^{0.4}$ in the correlation between the average ion charge state $\bar{z}$ and kinetic energy E in the expansion of laser-driven tin plasma. Our observation is explained from a simple analytical relation supported by a radiation-hydrodynamic simulation of an expanding laser-driven plasma. The analytical approach indicates that power-law behavior is expected from laser-produced tin plasma over a wide range of experimental parameters, which is strongly supported by data taken from numerous experiments including those of CO_2-laser-driven plasmas of relevance to the industrial setting. Identical power-law type behavior is generically predicted for dense, laser-driven plasma from a wide range of elements that are relevant for current and future laser-driven plasma light sources. We may further generalize to expect power-law relations between average charge state and kinetic energy for plasmas that are sufficiently dense containing ions with complex structures, i.e., open-shell atomic systems. This enables the prediction of the scaling of ion energies over a wide range of applications and separately simplifies the operation of complex ion charge-energy detectors after having established the sole prefactor in the power-law relation. We may expect departures from the power-law relation in the case of departures of the underlying $\bar{z} \propto T^{\alpha}$ scaling, for example near closed atomic subshells. Non-LTE conditions may separately lead to deviations; however, the existence of effective temperatures [69–71] may extend the validity of the power-law relation to such conditions.

Acknowledgments—Part of this work was conducted at the Advanced Research Center for Nanolithography (ARCNL), a public-private partnership between the University of Amsterdam (UvA), Vrije Universiteit Amsterdam (VU), the University of Groningen (UG), the Netherlands Organization for Scientific Research (NWO), and the semiconductor equipment manufacturer ASML. This project has received funding from the European Research Council (ERC) under the European Union's Horizon 2020 research and innovation program under Grant Agreement No. 802648. This work made use of the Dutch national *e*-infrastructure with the support of the SURF Cooperative using Grant No. EINF-2947.

[1] A. Higginson, R. J. Gray, M. King, R. J. Dance, S. D. R. Williamson, N. M. H. Butler, R. Wilson, R. Capdessus, C. Armstrong, and J. S. Green *et al.*, Nat. Commun. **9**, 724 (2018).
[2] M. Rehwald, S. Assenbaum, C. Bernert, F.-E. Brack, M. Bussmann, T. E. Cowen, C. B. Curry, F. Fiuza, M. Garten, L. Gaus *et al.*, Nat. Commun. **14**, 4009 (2023).
[3] A. Macchi, M. Borghesi, and M. Passoni, Rev. Mod. Phys. **85**, 751 (2013).
[4] M. Roth, T. E. Cowan, M. H. Key, S. P. Hatchett, C. Brown, W. Fountain, J. Johnson, D. M. Pennington, R. A. Snavely, S. C. Wilks *et al.*, Phys. Rev. Lett. **86**, 436 (2001).
[5] P. K. Patel, A. J. Mackinnon, M. H. Key, T. E. Cowan, M. E. Foord, M. Allen, D. F. Price, H. Ruhl, P. T. Springer, and R. Stephens, Phys. Rev. Lett. **91**, 125004 (2003).
[6] S. V. Bulanov and V. S. Khoroshkov, Plasma Phys. Rep. **28**, 453 (2002).
[7] S. Bulanov, T. Esirkepov, V. Khoroshkov, A. Kuznetsov, and F. Pegoraro, Phys. Lett. A **299**, 240 (2002).
[8] P. M. Nilson, L. Willingale, M. C. Kaluza, C. Kamperidis, S. Minardi, M. S. Wei, P. Fernandes, M. Notley, S. Bandyopadhyay, M. Sherlock *et al.*, Phys. Rev. Lett. **97**, 255001 (2006).
[9] F. Gobet, M. Comet, J.-R. Marquès, V. Méot, X. Raymond, M. Versteegen, J.-L. Henares, and O. Morice, Phys. Rev. E **98**, 063202 (2018).
[10] M. Comet, M. Versteegen, F. Gobet, D. Denis-Petit, F. Hannachi, V. Meot, and M. Tarisien, J. Appl. Phys. **119**, 013301 (2016).
[11] D. M. Packwood, S. Shiraki, and T. Hitosugi, Phys. Rev. Lett. **111**, 036101 (2013).
[12] B. Shin and M. J. Aziz, Phys. Rev. B **76**, 085431 (2007).
[13] S. I. Anisimov, D. Bäuerle, and B. S. Luk'yanchuk, Phys. Rev. B **48**, 12076 (1993).
[14] S. Fujioka, H. Nishimura, K. Nishihara, M. Murakami, Y.-G. Kang, Q. Gu, K. Nagai, T. Norimatsu, N. Miyanaga, Y. Izawa *et al.*, Appl. Phys. Lett. **87**, 241503 (2005).
[15] J. Beckers, T. H. M. van de Ven, C. A. de Meijere, R. M. van der Horst, M. van Kampen, and V. Y. Banine, Appl. Phys. Lett. **114**, 133502 (2019).
[16] O. O. Versolato, Plasma Sources Sci. Technol. **28**, 083001 (2019).
[17] I. Fomenkov, D. Brandt, A. Ershov, A. Schafgans, Y. Tao, G. Vaschenko, S. Rokitski, M. Kats, M. Vargas, M. Purvis *et al.*, Adv. Opt. Technol. **6**, 173 (2017).
[18] A. O'Connor, O. Morris, and E. Sokell, J. Appl. Phys. **109**, 073301 (2011).
[19] A. Z. Giovannini, N. Gambino, B. Rollinger, and R. S. Abhari, J. Appl. Phys. **117**, 033302 (2015).
[20] L. Poirier, D. J. Hemminga, A. Lassise, L. Assink, R. Hoekstra, J. Sheil, and O. O. Versolato, Phys. Plasmas **29**, 123102 (2022).
[21] D. Nakamura, K. Tamaru, Y. Hashimoto, T. Okada, H. Tanaka, and A. Takahashi, J. Appl. Phys. **102**, 123310 (2007).
[22] D. Bleiner and T. Lippert, J. Appl. Phys. **106**, 123301 (2009).
[23] D. B. Abramenko, M. V. Spiridonov, P. V. Krainov, V. M. Krivtsun, D. I. Astakhov, V. V. Medvedev, M. van Kampen,

D. Smeets, and K. N. Koshelev, Appl. Phys. Lett. **112**, 164102 (2018).
[24] S. Rai, K. I. Bijlsma, L. Poirier, E. de Wit, L. Assink, A. Lassise, I. Rabadán, L. Méndez, J. Sheil, O. O. Versolato *et al.*, Plasma Sources Sci. Technol. **32**, 035006 (2023).
[25] A. Elsied, N. Termini, P. Diwakar, and A. Hassanein, Sci. Rep. **6**, 38256 (2016).
[26] D. Wu, X. Mao, G. Chan, R. Russo, V. Zorba, and H. Ding, J. Anal. At. Spectrom. **35**, 767 (2020).
[27] D. J. Hemminga, L. Poirier, M. M. Basko, R. Hoekstra, W. Ubachs, O. O. Versolato, and J. Sheil, Plasma Sources Sci. Technol. **30**, 105006 (2021).
[28] I. V. Roudskoy, Laser Part. Beams **14**, 369 (1996).
[29] R. A. Burdt, Y. Ueno, Y. Tao, S. Yuspeh, M. S. Tillack, and F. Najmabadi, Appl. Phys. Lett. **97**, 041502 (2010).
[30] G. J. Tallents, Plasma Phys. **22**, 709 (1980).
[31] R. Dinger, K. Rohr, and H. Weber, J. Phys. D **13**, 2301 (1980).
[32] S. A. Abbasi, M. S. Hussain, B. Ilyas, M. Rafique, A. H. Dogar, and A. Qayyum, Laser Part. Beams **33**, 81 (2015).
[33] S. Kondrashev, T. Kanesue, M. Okamura, and K. Sakakibara, J. Appl. Phys. **100**, 103301 (2006).
[34] Y. Y. Tsui, R. Fedosejevs, A. A. Offenberger, R. Rankin, and C. E. Capjack, Phys. Fluids B **5**, 4115 (1993).
[35] P. Écija, M. N. Sánchez Rayo, R. Martínez, B. Sierra, C. Redondo, F. J. Basterretxea, and F. Castaño, Phys. Rev. A **77**, 032904 (2008).
[36] X. Wang, S. Zhang, X. Cheng, E. Zhu, W. Hang, and B. Huang, Spectrochim. Acta Part B **99**, 101 (2014).
[37] R. S. Abhari, B. Rollinger, A. Z. Giovannini, O. Morris, I. Henderson, and S. S. Ellwi, J. Micro/Nanolithogr., MEMS, MOEMS **11**, 021114 (2012).
[38] L. Poirier, A. Lassise, R. Hoekstra, J. Sheil, and O. O. Versolato, Phys. Plasmas **30**, 083505 (2023).
[39] L. Poirier, A. Lassise, Y. Mostafa, L. Behnke, N. Braaksma, L. Assink, R. Hoekstra, and O. O. Versolato, Appl. Phys. B **128**, 135 (2022).
[40] *Modern Methods in Collisional-Radiative Modeling of Plasmas*, edited by Y. Ralchenko (Springer International Publishing, Cham, 2016).
[41] R. M. More, Atoms in dense plasmas, in *Atoms in Unusual Situations*, edited by J. P. Briand (Springer US, Boston, MA, 1986), pp. 155–215.
[42] *High-Energy-Density Physics (Foundation of Inertial Fusion and Experimental Astrophysics)*, edited by R. P. Drake (Springer, Springer-Verlag Berlin Heidelberg, 2006).
[43] D. Salzmann, *Atomic Physics in Hot Plasmas* (Oxford University Press, New York, 1998).
[44] See Supplemental Material at http://link.aps.org/supplemental/10.1103/PhysRevLett.133.125101 for details on the Thomas-Fermi calculations and the experimental parameters (presented in Table S1) of the entries in Fig. 3., which includes Refs. [45–47].
[45] L. Behnke, R. Schupp, Z. Bouza, M. Bayraktar, Z. Mazzotta, R. Meijer, J. Sheil, S. Witte, W. Ubachs, R. Hoekstra *et al.*, Opt. Express **29**, 4475 (2021).
[46] R. Schupp, L. Behnke, Z. Bouza, Z. Mazzotta, Y. Mostafa, A. Lassise, L. Poirier, J. Sheil, M. Bayraktar, W. Ubachs *et al.*, J. Phys. D **54**, 365103 (2021).
[47] Y. Mostafa, L. Behnke, D. J. Engels, Z. Bouza, J. Sheil, W. Ubachs, and O. O. Versolato, Appl. Phys. Lett. **123**, 234101 (2023).
[48] M. M. Basko, V. G. Novikov, and A. S. Grushin, Phys. Plasmas **22**, 053111 (2015).
[49] J. Sheil, O. O. Versolato, V. Bakshi, and H. A. Scott, Atoms **11**, 130 (2023).
[50] M. Murakami and M. M. Basko, Phys. Plasmas **13**, 012105 (2006).
[51] M. M. Basko, J. Maruhn, and A. Tauschwitz, GSI Rep. **1**, 410 (2010).
[52] M. M. Basko, P. V. Sasorov, M. Murakami, V. G. Novikov, and A. S. Grushin, Plasma Phys. Control. Fusion **54**, 055003 (2012).
[53] A. Tauschwitz, M. Basko, A. Frank, V. Novikov, A. Grushin, A. Blazevic, M. Roth, and J. A. Maruhn, High Energy Density Phys. **9**, 158 (2013).
[54] F. Torretti, J. Sheil, R. Schupp, M. M. Basko, M. Bayraktar, R. A. Meijer, S. Witte, W. Ubachs, R. Hoekstra, O. O. Versolato *et al.*, Nat. Commun. **11**, 2334 (2020).
[55] S. Faik, A. Tauschwitz, and I. Iosilevskiy, Comput. Phys. Commun. **227**, 117 (2018).
[56] R. M. More, K. H. Warren, D. A. Young, and G. B. Zimmerman, Phys. Fluids **31**, 3059 (1988).
[57] A. J. Kemp and J. Meyer-ter-Vehn, Nucl. Instrum. Methods Phys. Res., Sect. A **415**, 674 (1998).
[58] B. Doggett and J. G. Lunney, J. Appl. Phys. **109**, 093304 (2011).
[59] M. Murakami, Y.-G. Kang, K. Nishihara, S. Fujioka, and H. Nishimura, Phys. Plasmas **12**, 062706 (2005).
[60] R. R. Goforth and P. Hammerling, J. Appl. Phys. **47**, 3918 (1976).
[61] N. R. Badnell, A. Foster, D. C. Griffin, D. Kilbane, M. O'Mullane, and H. P. Summers, J. Phys. B **44**, 135201 (2011).
[62] Y. B. Fu, C. Z. Dong, M. G. Su, F. Koike, G. O'Sullivan, and J. G. Wang, Phys. Rev. A **83**, 062708 (2011).
[63] S. S. Churilov, R. R. Kildiyarova, A. N. Ryabtsev, and S. V. Sadovsky, Phys. Scr. **80**, 045303 (2009).
[64] T. Otsuka, D. Kilbane, J. White, T. Higashiguchi, N. Yugami, T. Yatagai, W. Jiang, A. Endo, P. Dunne, and G. O'Sullivan, Appl. Phys. Lett. **97**, 111503 (2010).
[65] D. Kilbane and G. O'Sullivan, J. Appl. Phys. **108**, 104905 (2010).
[66] T. Higashiguchi, T. Otsuka, N. Yugami, W. Jiang, A. Endo, B. Li, P. Dunne, and G. O'Sullivan, Appl. Phys. Lett. **100**, 014103 (2012).
[67] J. Wang, M. Kishimoto, T. Jozaki, T. Kumeda, T. Higashiguchi, A. Sunahara, H. Ohiro, K. Yamasaki, and S. Namba, Phys. Rev. E **107**, 065211 (2023).
[68] H. Ohashi, T. Higashiguchi, Y. Suzuki, G. Arai, Y. Otani, T. Yatagai, B. Li, P. Dunne, G. O'Sullivan, W. Jiang *et al.*, Appl. Phys. Lett. **104**, 234107 (2014).
[69] M. Busquet, Phys. Fluids B **5**, 4191 (1993).
[70] J. Bauche and C. Bauche-Arnoult, J. Phys. B **33**, L283 (2000).
[71] J. Sheil, O. O. Versolato, A. J. Neukirch, and J. Colgan, J. Phys. B **54**, 035002 (2021).